

The contribution of red dwarfs and white dwarfs to the halo dark matter

S. Torres^{1,2}, J. Camacho¹, J. Isern^{3,2} and E. García-Berro^{1,2}

¹ Departament de Física Aplicada, Escola Politècnica Superior de Castelldefels, Universitat Politècnica de Catalunya, Avda. del Canal Olímpic 15, 08860 Castelldefels, Spain

² Institute for Space Studies of Catalonia, c/Gran Capità 2–4, Edif. Nexus 104, 08034 Barcelona, Spain

³ Institut de Ciències de l’Espai, CSIC, Campus UAB, Facultat de Ciències, Torre C-5, 08193 Bellaterra, Spain

November 19, 2018

ABSTRACT

Context. The nature of the several microlensing events observed by the MACHO team towards the LMC still remains controversial. Low-mass substellar objects and stars with masses larger than $\sim 1 M_{\odot}$ have been ruled out as major components of a MACHO galactic halo, while stars of half solar masses are the most probable candidates.

Aims. In this paper we assess jointly the relative contributions of both red dwarfs and white dwarfs to the mass budget of the galactic halo.

Methods. In doing so we use a Monte Carlo simulator which incorporates up-to-date evolutionary sequences of both red dwarfs and white dwarfs as well as detailed descriptions of our Galaxy and of the LMC. We explore the complete mass range between 0.08 and $1 M_{\odot}$ as possible microlensing candidates and we compare the synthetic populations obtained with our simulator with the results obtained by the MACHO and EROS experiments.

Results. Our results indicate that, despite that the contribution of the red dwarf population increases by a factor of 2 the value of the optical depth obtained when taking into account the white dwarf population alone, it is still insufficient to explain the number of events claimed by the MACHO team.

Conclusions. Finally, we find that the contribution to the halo dark matter of the whole population under study is smaller than 10% at the 95% confidence level.

Key words. stars: red dwarfs — stars: white dwarfs — stars: luminosity function, mass function — Galaxy: stellar content — Galaxy: stellar content — Galaxy: structure — Galaxy: halo

1. Introduction

Several cosmological observations show compelling evidence that baryons represent only a small fraction of the total matter in our Universe and that non-baryonic dark matter dominates over baryons. Within the standard cosmological model this naturally leads to the existence of a sort of unknown energy, the dark energy, which is the predominant component, $\Omega_{\Lambda} \simeq 0.72$, along with the dark matter component, $\Omega_{\text{M}} \simeq 0.27$, whereas the baryonic component is just $\Omega_{\text{B}} \simeq 0.044$. Moreover, most of the baryons are non-luminous, since $\Omega_{\star} \simeq 0.005$. For the case of our own Galaxy it has been found that the virial mass out to 100 kpc is $M \approx 10^{12} M_{\odot}$ while the baryonic mass in the form of stars is $M_{\star} \approx 7 \times 10^{10} M_{\odot}$, which means that for the Milky Way, the baryon fraction is at most 8% (Klypin et al. 2007). This problem is known as the missing baryon problem — see the review of Silk (2007) for a complete, interesting and recent discussion of this issue — and it is critical in our understanding of how the Galaxy (an by extension other galaxies) were formed and will ultimately evolve. To solve this problem, three alternatives can be envisaged: either these baryons are in the outer regions of our Galaxy, or, perhaps, they never were present in the protogalaxy or, finally, they may have been ejected from the Milky Way. The most promising explanation and the currently favored one is the first of these options.

Since the pioneering proposal of Paczyński (1986) that gravitational microlensing could be used to clarify the nature of galactic dark matter, considerable observational and theoretical efforts have invested in this issue. Among the most likely candidates for building up the baryonic dark matter density are massive baryonic halo objects, or MACHOs. From the theoretical point of view it has been suggested that MACHOs could be planets ($M \sim 10^{-7} M_{\odot}$), brown and red dwarfs (with masses ranging from ~ 0.01 to $\sim 1 M_{\odot}$), primordial black holes ($M \gtrsim 10^{-16} M_{\odot}$), molecular clumps ($M \sim 1 M_{\odot}$) and old white dwarfs ($M \sim 0.6 M_{\odot}$). From the observational perspective the MACHO (Alcock et al. 1997, 2000), EROS (Lasserre et al. 2001; Goldman et al. 2002; Tisserand et al. 2007), OGLE (Udalski et al. 1994), MOA (Muraki et al. 1999) and SuperMACHO (Becker et al. 2005) teams have monitored millions of stars during several years in both the Large Magellanic Cloud (LMC) and the Small Magellanic Cloud (SMC) to search for microlensing events. However, only the MACHO team and the EROS group have reported their results. Despite that initially some divergences appeared between their results, agreement has been reached in some important points. For instance, no microlensing candidates have been found by the MACHO team or the EROS group with event durations between a few hours and 20 days. This means that the Galactic halo could contain no more than a 10% of dark objects in the mass range $10^{-7} < M/M_{\odot} < 10^{-3}$. This rules out planets and brown dwarfs as the major contributors to the mass budget of the dark halo. Moreover the MACHO collabora-

tion has succeeded in revealing ~ 15 microlensing events during their 5.7 yr analysis of 11.9 million stars in the LMC (Alcock et al. 2000). In their analysis they derived an optical depth towards the LMC of $\tau = 1.2_{-0.3}^{+0.4} \times 10^{-7}$ or, equivalently, an halo fraction $0.08 < f < 0.50$ at the 95% confidence level with a MACHO mass in the range $0.15 \leq M/M_{\odot} \leq 0.50$, depending on the halo model. On the other hand, the negative results found by the EROS collaboration provide an upper limit. Specifically, the EROS team has presented an analysis of a subsample of bright stars belonging to the LMC (Tisserand et al. 2007), in order to minimize the source confusion and blending effects. Their results imply that the optical depth towards the LMC is $\tau < 0.36 \times 10^{-7}$ at the 95% confidence level, corresponding to a fraction of halo mass of less than 7%. This result is 4 times smaller than that obtained by the MACHO team. Consequently, further discussion has been opened concerning the location and nature of the lenses. In particular, recent LMC models have been used in order to ascertain if possible asymmetries in the space distribution of the microlensed stars are assimilable to Galactic halo objects or LMC ones. In fact, different studies show that a sizeable fraction of the microlensed events are due to LMC self-lensing (Sahu 1994; Gyuk, Dalal & Griest 2000; Calchi Novati et al. 2006). Moreover, a full variety of possible explanations have been proposed to reproduce the microlensing events: tidal debris or a dwarf galaxy toward the LMC (Zhao 1998), a Galactic extended shroud population of white dwarfs (Gates & Gyuk 2001), blending effects (Belokurov, Evans & Le Du 2003, 2004), spatially varying mass functions (Kerins & Evans 1998, Rahvar 2005), and other explanations (Holopainen et al. 2006). However, all of these proposals have been received with some criticism because none of them fully explains the observed microlensing results.

Other observational pieces of evidence are added to conform the present puzzle, such as the search for very faint objects in the Hubble Deep Field or the search for the microlensing events towards the Galactic bulge or towards very crowded fields like M31. Particularly, the Hubble Deep Field has provided us with an opportunity to test the contribution of white dwarfs to the Galactic dark matter. Ibata et al. (1999) and, most recently, Kilic et al. (2005) have claimed the detection of some white dwarf candidates among several faint blue objects. These objects exhibit significant proper motion and, thus, are assumed to belong to the thick disk or the halo populations. Despite the increasing number of surveys searching for white dwarfs — like the Sloan Digital Sky Survey (Eisenstein et al. 2006), the 2 Micron All Sky Survey (Cutri et al. 2003), the SuperCosmos Sky Survey (Hambly, Irwin & MacGillivray 2001), the 2dF QSO Redshift Survey (Vennes et al. 2002), and other observational searches (Knox et al. 1999; Ibata et al. 1999; Oppenheimer et al. 2001; Majewski & Siegel 2002; Nelson et al. 2002) — and the numerous theoretical studies (Isern et al. 1998; Reylyé et al. 2001; Flynn et al. 2003; Hansen & Liebert 2003; García-Berro et al. 2004), the problem still remains open. In addition, despite the fact that, for obvious reasons, no information about the halo could be derived from the microlensing events towards the Galactic bulge, the results obtained so far indicate the primordial role played by low-mass stars rather than other objects.

In two previous papers we have extensively analyzed the role played by the carbon–oxygen (CO) white dwarf population (García-Berro et al. 2004) as well as the contribution of oxygen–neon (ONe) white dwarfs (Camacho et al. 2007). In these papers we have performed a thorough study of a wide range of Galactic inputs, including different initial mass functions and halo ages, and several density profiles corresponding to differ-

ent halo models. The calculations reported in these two papers have shown that a sizeable fraction of the halo dark matter cannot be locked in the form of white dwarfs. Specifically, we have found that this contribution is of the order of a modest 5% in the most optimistic case, that it is mainly due to old CO white dwarfs with hydrogen–rich atmospheres and that the contribution of ONe white dwarfs is minor, because although ONe white dwarfs can reach faint magnitudes faster than CO white dwarfs, their contribution is heavily suppressed by the initial mass function.

In this paper we analyze in a comprehensive way a wide range of masses $0.08 < M/M_{\odot} < 10$ susceptible to produce microlensing events towards the LMC and, thus, to contribute to the halo dark matter. The full range of masses studied here represents nearly the 90% of the stellar content, including the red dwarf regime ($M > 0.075 M_{\odot}$) the CO white dwarf population and the population of massive ONe white dwarfs. The paper is organized as follows. In Sect. 2 we summarize the main ingredients of our Monte Carlo code and other basic assumptions and procedures necessary to evaluate the microlensing optical depth towards the LMC. Section 3 is devoted to describe our main results, including the contribution of red dwarfs and white dwarfs to the microlensing optical depth towards the LMC, and we compare our results to those of the MACHO and EROS teams. In this section we also estimate the probability that a microlensing event could be assigned to one or another of the populations under study and we discuss the contribution of red and white dwarfs to the baryonic content of the Galaxy. Finally, in Sect. 4 our major findings are summarized and we draw our conclusions.

2. The model

2.1. Building the sample

A detailed description of our Monte Carlo simulator has been already presented in Torres et al. (2002), García-Berro et al. (2004) and Camacho et al. (2007). Therefore, we will only summarize here the most important inputs. The basic ingredient of any Monte Carlo simulator is a random number generator algorithm which must ensure a non-correlated sequence and a good set of statistical properties. We have used a random number generator algorithm (James 1990) which provides a uniform probability density within the interval (0, 1) and ensures a repetition period of $\gtrsim 10^{18}$, which is enough for our purposes. Each one of the Monte Carlo simulations presented here consists of an ensemble of $\sim 5 \times 10^4$ independent realizations of the synthetic star population, for which the average of any observational quantity along with its corresponding standard deviation were computed. Here the standard deviation means the ensemble mean of the sample dispersions for a typical sample.

The galactic halo has been modelled assuming a spherically symmetric halo. In particular the model used here is the typical isothermal sphere of radius 5 kpc also called the “S-model”, which has been extensively used by the MACHO collaboration (Alcock et al. 2000; Griest 1991). The position of each synthetic star is randomly chosen according to this density profile. We have not used other profiles, such as the exponential power-law model, the Navarro, French & White (1997) density profile and others because their inclusion in the analysis presented here does not provide significant variations in the final results (García-Berro et al. 2004). Likewise, this reasoning is extensible to the non-standard galactic halo models, such as flattened profiles, oblate halo models, and others, which are beyond the scope of the present study.

The mass distribution of synthetic stars has been computed according to two different initial mass functions, the standard initial mass function of Scalo (1998) and the biased log–normal initial mass function proposed by Adams & Laughlin (1996), the later being representative of other non–conventional initial mass functions such as the one of Chabrier et al. (1996). Note, however, that these biased initial mass functions seem to be incompatible with the observed properties of the halo white dwarf population (Isern et al. 1998; García–Berro et al. 2004), with the contribution of thermonuclear supernovae to the metallicity of the Galactic halo (Canal et al. 1997), and with the observations of galactic halos in deep galaxy surveys (Charlot & Silk 1995). Nevertheless, for the sake of completeness, we prefer to include in the present analysis a representative example of these biased mass function in order to illustrate the role played by the red dwarf population when a biased initial mass function is adopted.

The main sequence mass is obtained by drawing a pseudo–random number according to the adopted initial mass function. The time at which a star was born is randomly chosen, previously assuming that the halo was formed 14 Gyr ago in an intense burst of star formation of duration ~ 1 Gyr. The main–sequence lifetime as a function of the mass in the main sequence is that of Iben & Laughlin (1989). Once the mass of a synthetic star is chosen, the main–sequence lifetime is obtained and from it we know which stars are able to evolve to white dwarfs or which ones remain in the main sequence as red dwarfs. We have considered red dwarfs to have masses in the range $0.08 < M/M_{\odot} < 1$. For these stars we have adopted the evolutionary models of Baraffe et al. (1998). Stars with such small masses have very large main–sequence lifetimes. Consequently, no post–main–sequence evolutionary tracks of these stars were needed. For those stars which have had time enough to enter in the white dwarf cooling track, and given a set of theoretical cooling sequences and the initial to final mass relationship (Iben & Laughlin 1989) their luminosities, effective temperatures and colors were obtained. The cooling sequences adopted here depend on the mass of the white dwarf. White dwarfs with masses smaller than $M_{\text{WD}} = 1.1 M_{\odot}$ are expected to have a CO core and, consequently, we adopt for them the cooling tracks of Salaris et al. (2000). White dwarfs with masses larger than $M_{\text{WD}} = 1.1 M_{\odot}$ most probably have ONe cores and for these white dwarfs we adopt the most recent cooling sequences of Althaus et al. (2007). Both sets of cooling sequences incorporate the most accurate physical inputs for the stellar interior (including neutrinos, crystallization, phase separation and Debye cooling) and reproduce the blue turn at low luminosities (Hansen 1998).

The kinematical properties of the halo population have been modeled according to gaussian laws (Binney & Tremaine 1987) with radial and tangential velocity dispersions accordingly related by the Jean’s equation and fulfilling the flat rotation curve of our Galaxy. We have adopted standard values for the circular velocity $V_c = 220$ km/s as well as for the peculiar velocity of the Sun $(U_{\odot}, V_{\odot}, W_{\odot}) = (10.0, 15.0, 8.0)$ km/s (Dehnen & Binney 1998). Additionally, we have discarded those stars with velocities smaller than 250 km/s given that they are not considered as halo members. Besides we have rejected stars with velocities larger than 750 km/s, because they would have velocities exceeding 1.5 times the escape velocity. Finally, since white dwarfs usually do not have determinations of the radial component of the velocity, the radial velocity is eliminated when a comparison with the observational data is needed.

Finally, and in order to compare the simulated results with the observational ones, a normalization criterion should be used. We have proceeded as in our previous papers (Camacho et al.

2007; García–Berro et al. 2004). That is, we have normalized our simulations to the local density of halo white dwarfs obtained from the halo white dwarf luminosity function of Torres et al. (1998) taking into account the new halo white dwarf candidates in the SDSS Stripe 82 (Vidrih et al. 2007).

2.2. The LMC microlensing model

In order to mimic the microlensing experiments towards the LMC we have simulated it following closely the detailed LMC descriptions of Gyuk et al. (2000) and Kallivayalil et al. (2006). Our model takes into account, among other parameters, the scale length and scale height of the LMC, its inclination and its kinematical properties. This model provides us with a synthetic population of stars representative of the monitored point sources. Afterwards we have evaluated which star of the galactic halo could be responsible of a microlensing event. We have only considered stars fulfilling a series of conditions. First of all the lensing star should be fainter than a certain magnitude limit. In a second step we have checked if the lens is inside the Einstein tube of the monitored star. That is, if the angular distance between the lens and monitored star is smaller than the Einstein radius. We recall here that the Einstein radius is given by

$$R_E = 2 \sqrt{\frac{GMD_{\text{OS}}}{c^2} x(1-x)} \quad (1)$$

where D_{OS} is the observer–source distance and $x \equiv D_{\text{OL}}/D_{\text{OS}}$. Finally, we filter those stars which are candidates to produce a microlensing event with the detection efficiency function, $\varepsilon(\hat{t}_i)$, where \hat{t}_i is the Einstein ring diameter crossing time. The detection efficiency depends on the particular characteristics of the experiment. In our case we have reproduced the MACHO and EROS experiments. Specifically, for the MACHO collaboration we have taken 1.1×10^7 stars during 5.7 yr and over 13.4 deg^2 , whereas the detection efficiency has been modelled according to:

$$\varepsilon(\hat{t}) = \begin{cases} 0.43 e^{-(\ln(\hat{t}/T_m))^{3.58}/0.87}, & \hat{t} > T_m \\ 43 e^{-|\ln(\hat{t}/T_m)|^{2.34}/11.16}, & \hat{t} < T_m \end{cases} \quad (2)$$

where $T_m = 250$ days. This expression provides a good fit to the results of Alcock et al. (2000). For the EROS experiment we have used 0.7×10^7 stars over a wider field of 84 deg^2 and over a period of 6.7 yr. Regarding the detection efficiency we have adopted a numerical fit to the results of Tisserand et al. (2007).

For all the simulations presented here we extract the parameters relevant to characterize the microlensing experiments. A complete description of the various parameters which have importance in discussing gravitational microlensing can be found in Mollerach & Roulet (2002) and Schneider et al. (2004). Among these parameters perhaps the most important one for our purposes is the optical depth, τ , which measures the probability that at a given time a star is magnified by a lens by more than a factor of 1.34. From an observational point of view an estimate of this parameter can be obtained using the expression (Alcock et al. 2000):

$$\tau = \frac{1}{E} \frac{\pi}{4} \sum_i \frac{\hat{t}_i}{\varepsilon(\hat{t}_i)} \quad (3)$$

where E is the total exposure in star–years. The optical depth is independent of the lens motion and mass distribution. However, since the experiments measure the number of events and their

durations, additional information can be obtained using the microlensing rate, Γ , and its distribution as function of the event durations. This parameter represents nothing else but the flux of lenses inside the microlensing tube. Finally, an estimate of the expected number of events can be done using the expression

$$N_{\text{exp}} = E \int_0^{\infty} \frac{d\Gamma}{dt} \varepsilon(\hat{t}_i) d\hat{t}_i \quad (4)$$

3. Results

3.1. Optical depth towards the LMC

As previously mentioned, the optical depth provides us with the most immediate and simplest information about the microlensing experiments. Even so, the optical depth plays a key point in our analysis since it provides us with rich information about the Galactic halo and the role of the dark matter. We will compare here the results obtained using our Monte Carlo simulator with those obtained by the MACHO collaboration. In Fig. 1 we show the contribution to the optical depth of the different simulated populations for the two initial mass functions under study as a function of the adopted magnitude cut. Our simulations have been normalized to the value derived by Alcock et al. (2000), $\tau_0 = 1.2 \times 10^{-7}$. The white dwarf populations are represented by solid and open squares for the CO and ONe white dwarfs, respectively. Open triangles show the contribution of red dwarfs, while the contribution of the three populations is represented by open circles. The first remarkable result is that for the standard initial mass function (top panel of Fig. 1) the combined contribution of red dwarfs and white dwarfs is at most one third of the observed optical depth and this is obtained when a totally unrealistic magnitude cut is adopted, $m_V \sim 15^{\text{mag}}$. Note as well that there is a clearly decreasing trend as the adopted magnitude cut increases. This can be easily understood, since fewer objects contribute to the optical depth as the magnitude cut increases. Furthermore, the slope is different for the three types of objects considered here. For instance, the contribution of red dwarfs decreases faster than the contribution of CO white dwarfs as the magnitude cut increases which, in turn, decreases faster than the contribution of ONe white dwarfs. This reflects the fact that, in general, red dwarfs are brighter than regular CO white dwarfs. Finally, ONe white dwarfs cool very fast (Althaus et al. 2007) and thus, for realistic halo ages, are faint objects. Consequently, their contribution remains almost constant. It is interesting to note as well that the optical depth obtained for the whole population almost doubles that obtained when only the white dwarf population is taken into account. However, in agreement with other studies, the value obtained here still remains far below the observed one and it is thus clear that the Galactic halo population is not enough to explain the results of the MACHO team. Even the alternative initial mass functions, of which that of Adams & Laughlin (1996) is a representative example, predict that $\langle \tau / \tau_0 \rangle$ is, in the best of the cases, 0.3 and this happens for unrealistic magnitude cuts — see the bottom panel of Fig. 1. The results obtained using the non-standard initial mass function deserve two additional comments. In particular, it is interesting to note that the largest contribution in this case is that of the CO white dwarf population and, secondly, that the contribution of red dwarfs is totally negligible for magnitude cuts larger than $m_V \sim 23^{\text{mag}}$, which is a reasonable value for current surveys. Both facts are natural since this initial mass function has been tailored to produce a large population of $0.5 M_{\odot}$ white dwarfs. In summary, the fraction of the microlensing optical depth which a stellar halo

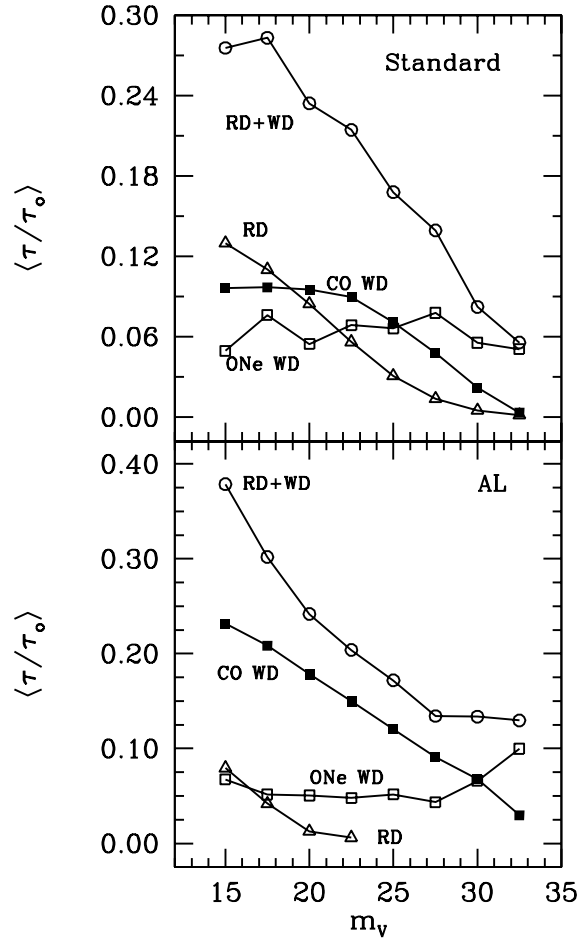


Fig. 1. Microlensing optical depth towards the LMC as a function of the limiting magnitude. Solid and open squares represent the CO and ONe white dwarf populations, respectively. Red dwarfs are represented using open triangles, while the whole population is shown using open circles.

can account for in the range of masses under study here is at most one third of that observed by the MACHO team, independently of the adopted initial mass function.

In Table 1 we have summarized the average values for the different parameters of the whole population for the two initial mass functions under study and for four magnitude cuts. Specifically, in Table 1 we present the number of microlensing events, the average mass of the microlenses, their average proper motion, distance and tangential velocity, the corresponding Einstein crossing times and, finally, the contribution to the microlensing optical depth. It is clear that some of these parameters are to some extent dependent of the magnitude cut. For instance, the average distance of the sample increases as the magnitude cut is larger. This is a natural consequence of selecting more distant objects which, in turn, implies longer Einstein crossing times. This behavior is independent of the assumed initial mass function. However, there are characteristics which do not change as the magnitude cut increases. For instance, this is the case of the expected number of events or the average mass of the sample. In the case of a standard initial mass function no more than one microlensing event should be expected at the 1σ confidence level, while for a log-normal mass function up to 5 events might be expected. In any case the expected number

Magnitude	Standard				AL			
	17.5	22.5	27.5	32.5	17.5	22.5	27.5	32.5
$\langle N_{\text{WD}} \rangle$	0 ± 1	0 ± 1	0 ± 1	0 ± 1	3 ± 2	2 ± 1	1 ± 1	0 ± 1
$\langle m \rangle (M_{\odot})$	0.421	0.411	0.427	0.443	0.638	0.636	0.640	0.684
$\langle \mu \rangle ('' \text{ yr}^{-1})$	0.020	0.017	0.008	0.004	0.036	0.025	0.011	0.003
$\langle d \rangle (\text{kpc})$	2.48	3.79	6.62	13.08	1.39	2.15	5.13	19.6
$\langle V_{\text{tan}} \rangle (\text{km s}^{-1})$	240	247	262	241	240	252	263	261
$\langle \hat{t}_{\text{E}} \rangle (\text{d})$	41.2	49.3	63.3	82.8	34.7	46.6	76.4	126.8
$\langle \tau / \tau_0 \rangle$	0.283	0.214	0.139	0.055	0.302	0.204	0.140	0.129

Table 1. Summary of the results obtained for the whole simulated population of microlenses towards the LMC for an age of the halo of 14 Gyr, different model initial mass functions, and several magnitude cuts.

of microlensing events is far from the 17 events claimed by the MACHO experiment.

As already mentioned, the average mass of the microlenses depends on the initial mass function. To investigate this further in Fig. 2 the contribution to the optical depth as a function of the mass of the lens object for both initial mass functions is shown. The results obtained with our Monte Carlo simulator clearly show that for a standard initial mass function — top panel of Fig. 2 — there are two peaks centered at masses $\sim 0.3 M_{\odot}$ and $\sim 0.6 M_{\odot}$, respectively. These masses correspond to the average masses of red dwarfs and CO white dwarfs, respectively. Also noticeable is that the contribution of ONE white dwarfs can only be appreciated as an extended tail in the case of a standard initial mass function. This is in full agreement with recent studies about the distribution of masses of the white dwarf population (Finley et al. 1997; Liebert et al. 2005), which show the existence of a narrow sharp peak near $0.6 M_{\odot}$, with a tail extending towards larger masses, with several white dwarfs with spectroscopically determined masses within the interval comprised between 1.0 and $1.2 M_{\odot}$. The situation is different for the non-standard initial mass function, which is shown in the bottom panel of Fig. 2. The log-normal initial mass function considered here cannot produce red dwarfs with masses below $\sim 0.45 M_{\odot}$ and thus the peak at $0.3 M_{\odot}$ previously found is absent in this case.

A more detailed analysis of the role played by the red dwarf population can be done. To this end in Table 2 we have summarized the average values for the different parameters of the population of red dwarfs for both initial mass functions. Similar sets of data for the white dwarf population can be found in our previous studies (Camacho et al. 2007, García-Berro et al. 2004). As can be seen from Table 2, the red dwarf population roughly contributes a 10% to the observed MACHO optical depth for a standard initial mass function. It is also important to discuss the other parameters shown in Table 2. For instance, the average mass clearly decreases when the magnitude cut increases, which is the opposite to what occurs for the white dwarf population. This can be easily explained by taking into account that the more massive the red dwarf is the brighter is and, hence, we should expect less massive objects for larger magnitude cuts. This result is reinforced by the fact that the average distance increases for increasing magnitude cuts. Moreover, since the average tangential velocity remains constant, the combined effect of an average decreasing mass and an average increasing distance is that the Einstein crossing time remains practically constant. The characteristics of the red dwarf population are dramatically different when the initial mass function of Adams & Laughlin (1996) is used. In this case the production of low-mass red dwarfs is heavily suppressed. Accordingly, in our simulations we have not produced red dwarfs with masses smaller than $\sim 0.45 M_{\odot}$. Thus, since in average the masses are larger we also find brighter stars.

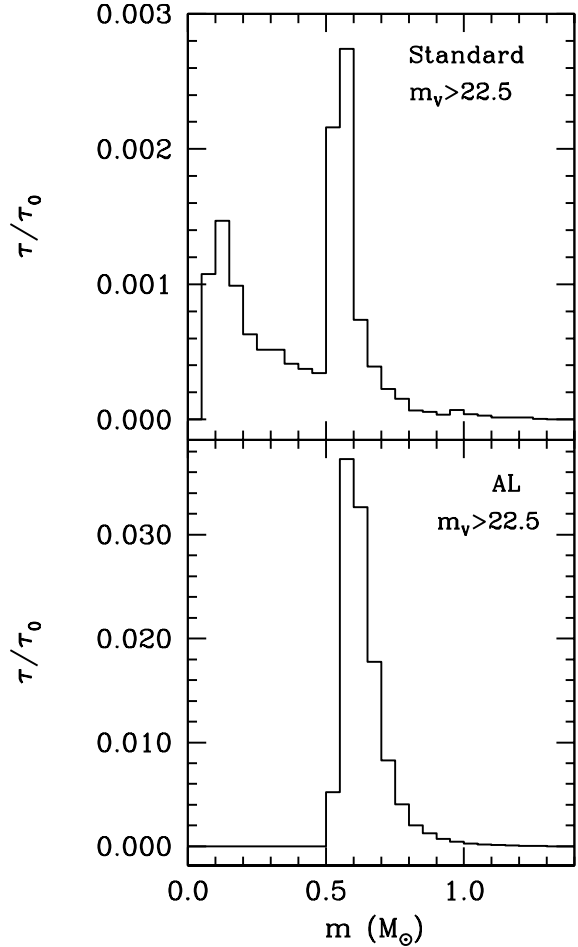


Fig. 2. Contribution to the optical depth as a function of the lens mass.

Hence, we expect no contribution at all for magnitude cuts above $m_v \approx 22.5^{\text{mag}}$, while for brighter magnitude cuts the average mass expected is $\sim 0.7 M_{\odot}$, which is even larger than the expected value for CO white dwarfs.

As already seen, for the standard initial mass function, a double-peaked profile is found, but the peak amplitude deserves a detailed analysis. The ratio of the contribution to the optical depth of a typical red dwarf with respect to the contribution of a typical CO white dwarf is

$$\frac{\tau_{\text{RD}}}{\tau_{\text{CO}}} = \frac{\hat{t}_{\text{RD}} \varepsilon(\hat{t}_{\text{CO}})}{\hat{t}_{\text{CO}} \varepsilon(\hat{t}_{\text{RD}})} \approx \sqrt{\frac{M_{\text{RD}} D_{\text{OL}}^{\text{RD}} \varepsilon(\hat{t}_{\text{CO}})}{M_{\text{CO}} D_{\text{OL}}^{\text{CO}} \varepsilon(\hat{t}_{\text{RD}})}} \quad (5)$$

Magnitude	Standard				AL			
	17.5	22.5	27.5	32.5	17.5	22.5	27.5	32.5
$\langle N_{\text{WD}} \rangle$	0 ± 1	0 ± 1	0 ± 1	0 ± 1	0 ± 1	0 ± 1	0 ± 0	0 ± 0
$\langle m \rangle (M/M_{\odot})$	0.324	0.228	0.119	0.092	0.747	0.622	—	—
$\langle \mu \rangle ('' \text{ yr}^{-1})$	0.018	0.011	0.006	0.005	0.010	0.002	—	—
$\langle d \rangle (\text{kpc})$	2.89	4.88	8.27	10.20	5.15	17.59	—	—
$\langle V_{\text{tan}} \rangle (\text{km s}^{-1})$	242	244	254	235	246	180	—	—
$\langle \hat{t}_{\text{E}} \rangle (\text{d})$	41.2	48.5	41.3	43.3	98.2	158.0	—	—
$\langle \tau/\tau_0 \rangle$	0.130	0.118	0.096	0.070	0.091	0.125	—	—

Table 2. Summary of the results obtained for the population of red dwarf microlenses towards the LMC for an age of the halo of 14 Gyr, different model initial mass functions, and several magnitude cuts.

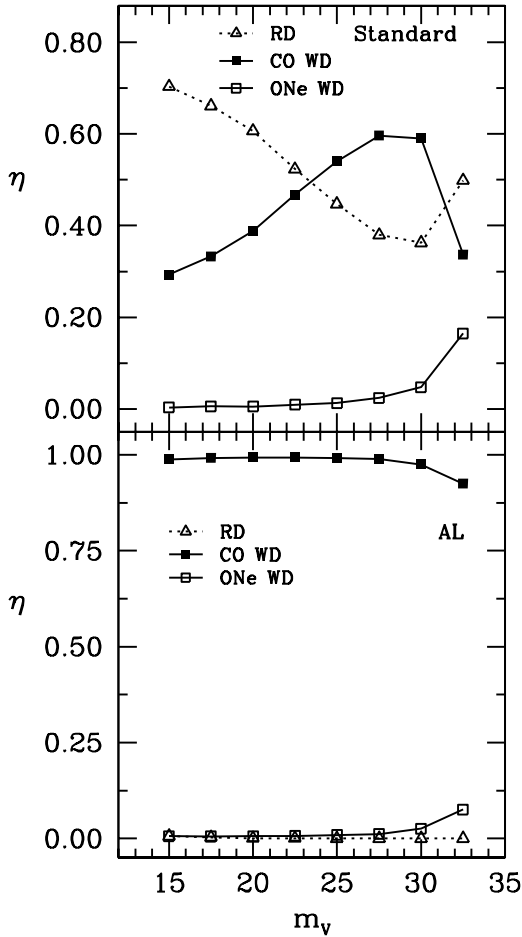


Fig. 3. Fraction of microlenses with respect to the whole population, as a function of the magnitude cut.

This value depends on the adopted initial mass function and on the magnitude cut used. For the standard initial mass function and a magnitude cut of 22.5^{mag} the average values of the mass and distance of a red dwarf are, respectively, $\sim 0.228 M_{\odot}$ and 4.88 kpc, while for a typical CO white dwarf the average mass is $\sim 0.568 M_{\odot}$ and the average distance is 3.14 kpc. With these values the ratio of the optical depths turns out to be $\tau_{\text{RD}}/\tau_{\text{CO}} \approx 0.9$. Thus, although the sample space of red dwarfs and white dwarfs is different the contribution to the optical depth per object results to be the same. For instance, the red dwarf population has a smaller average mass than white dwarfs but, conversely, the average distance is larger. Therefore, the total contribution of

these two populations results to be merely an account of the number of microlenses. In order to clarify this issue we have evaluated the fraction of microlenses due to the different populations as a function of the adopted magnitude cut. The results are shown in Fig. 3 for both the standard initial mass function — top panel — and the initial mass function of Adams & Laughlin (1996) — bottom panel. As it can be seen there, for the standard initial mass function the relative contribution of red dwarfs decreases with increasing magnitude cuts, while that of CO white dwarfs increases. Both contributions are equal for a magnitude cut of $\approx 24^{\text{mag}}$. Finally, the contribution of ONe white dwarfs remains roughly constant and only becomes appreciable for very large magnitude cuts. These trends can be attributed to the fact that red dwarfs are more numerous at bright magnitudes than white dwarfs, for which typical luminosities are of the order of $\log(L/L_{\odot}) \approx -3.5$. The situation is completely different when the log-normal initial mass function of Adams & Laughlin (1996) is used. As can be seen in the bottom panel of Fig. 3, the number of microlenses is practically dominated by the CO white dwarf contribution, while the contribution of red dwarfs and ONe white dwarfs is negligible.

3.2. The microlensing event rate

As previously pointed out, the contribution to the optical depth for a standard initial mass function is doubled when the red dwarf population is considered. We have also shown that for a standard initial mass function the contributions of red dwarfs and CO white dwarfs are roughly the same. Then, it is natural to ask ourselves if there are differences which can help us in discerning the contribution of one or another population using the observational data of the MACHO experiment. To assess this we have analyzed the microlensing rate as a function of the event duration. The results of our simulations for a standard initial mass function are shown in Fig. 4. Each of the panels is clearly labelled with the adopted magnitude cut and the population of microlenses. For the case of the left panels in Fig. 4 we have adopted a magnitude cut of 25^{mag} , whilst for the right panels a magnitude cut of 30^{mag} was adopted. In all the cases the simulated microlensing rate is shown using solid lines, while the observational data obtained by the MACHO team is shown using a dotted line. All the distributions are normalized to unit area. As can be seen, the red dwarf and the white dwarf distributions present some differences. For instance, for a magnitude cut of 25^{mag} it turns out that although both the red dwarf population and the white dwarf populations show a peak located at nearly ~ 20 days, the white dwarf population presents a wider distribution. In the case in which a magnitude cut of 30^{mag} is adopted the differences are more pronounced and it is clear that the peak of the distribution for the CO white population moves to longer

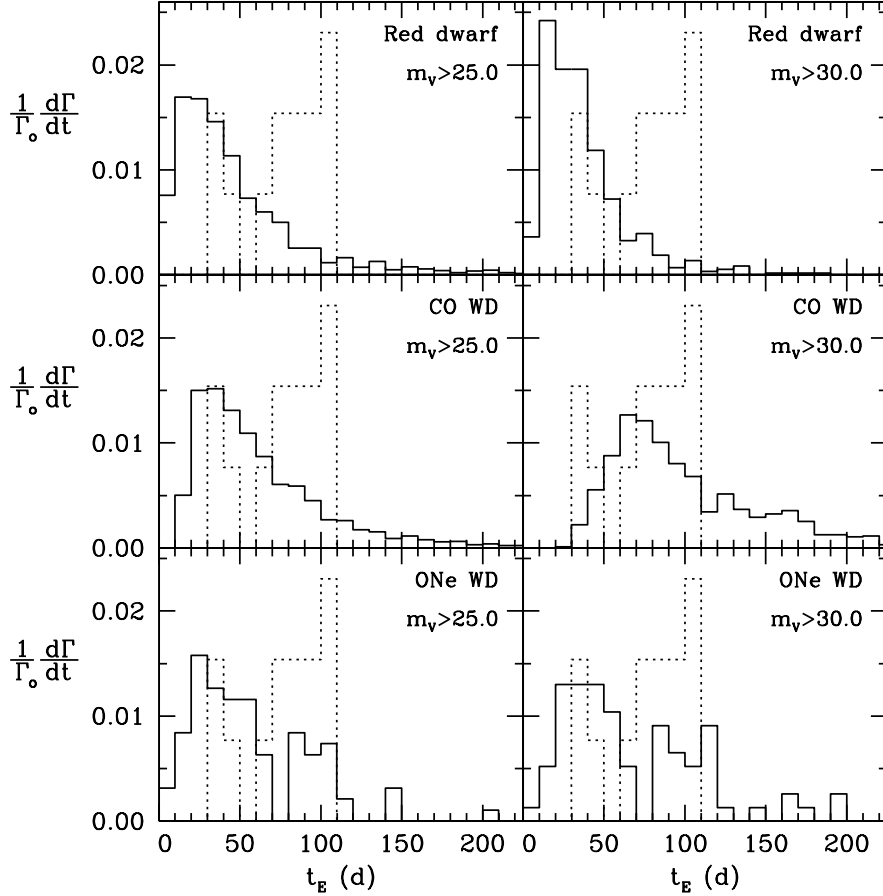


Fig. 4. Differential event rate normalized to unit area as a function of the Einstein crossing time for the populations under study and different magnitude cuts (solid lines). Also represented as a dotted line in each panel is the observational event distribution from Alcock et al. (2000).

Z^2 COMPATIBILITY TEST

Magnitude	17.5 ^{mag}	22.5 ^{mag}	25.0 ^{mag}	27.5 ^{mag}	30.0 ^{mag}
Red dwarfs	0.58	0.67	0.65	0.55	0.40
CO white dwarfs	0.61	0.70	0.80	0.87	0.90
ONe white dwarfs	0.76	0.55	0.68	0.68	0.72
Whole population	0.59	0.69	0.75	0.82	0.89

Table 3. Compatibility, as obtained using the Z^2 statistical test, of the observed MACHO distribution of Einstein crossing times and those of the different simulated populations.

durations (~ 70 days), whereas the peak of the red dwarf population does not move appreciably.

Additionally, and in order to make more quantitative estimates, we have performed a Z^2 statistical test of the compatibility of the different populations under study with the observed data. The Z^2 statistical test (Lucy 2000) represents an improvement over the standard χ^2 statistical test and it is especially designed for meagre data sets. In Table 3 we show the Z^2 probability of the different simulated populations being compatible with the distribution of Einstein times obtained by the MACHO experiment. It should be clarified that this probability represents an estimate of the degree to which the observed event rate distribution derives from a single population of stars. As can be seen in Table 3, the CO white dwarf population best matches the observational data, given that its compatibility is as high as 0.90 for the faintest magnitude cut. Moreover the compatibility of

this population with the observational data increases for fainter magnitude bins. In sharp contrast, the population of red dwarfs presents a decreasing trend as the magnitude cut increases and, additionally, the compatibility with the observational data is 0.70 in the best of the cases. With regard to the ONe white dwarf population the compatibility presents an almost constant value around 0.70, independently of the magnitude cut. These results indicate that the CO white dwarf population can reproduce the observed distribution of microlensing event rates. Even more, they dominate the behavior of the whole population, as can be seen by taking a look at the last row of Table 3, in which we analyze the compatibility of the whole population of simulated stars. Therefore, even if the expected number of microlensing events obtained in our simulations is considerably smaller than the ~ 15 events claimed by the MACHO team, the event rate distribution of the CO white dwarf population is in fair agreement

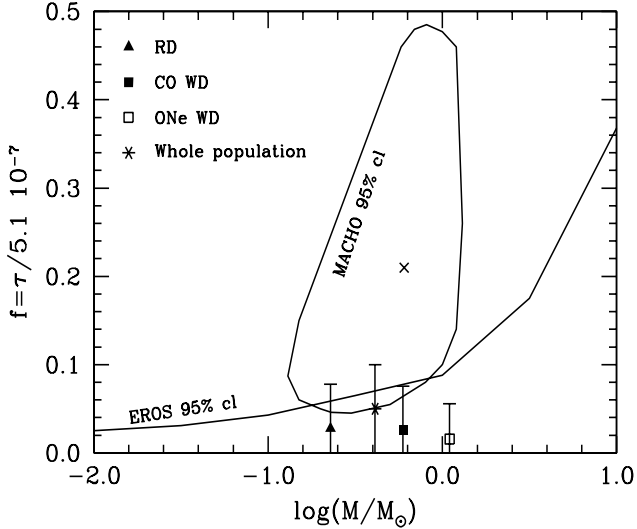


Fig. 5. Halo dark matter fraction as a function of the mass lens. Plotted using a solid line are the 95% confidence level curve for the MACHO experiment and the 95% confidence level upper limit for the EROS experiment.

with the observed distribution. This result puts into question to which extent we know the characteristics of the halo white dwarf population and if it exists other possible ways capable of producing a larger number of old white dwarfs in the stellar halo.

3.3. The EROS experiment

While the MACHO team claims for the identification up to 17 observed events, the EROS collaboration have not found any microlensing event towards the LMC and one candidate event towards the SMC. Adopting a standard halo model and assuming $\tau_{\text{SMC}} = 1.4\tau_{\text{LMC}}$, the EROS results imply an optical depth $\tau_0 = 0.36 \times 10^{-7}$ (Tisserand et al. 2007), which is four times smaller than that obtained by the MACHO team. We have also performed a set of simulations emulating the conditions of the EROS experiment with the same inputs previously described in Sect. 2. Although only minor differences should be expected in the analysis of the main results, it is clear as well that a joint study of both experiments using a controlled set of prescriptions represents a test of the robustness of our numerical procedure.

In Table 4 we have summarized the results obtained in this second set of Monte Carlo simulations of microlenses towards the LMC for the EROS experiment. Our simulations show that, for the standard initial mass function, the expected optical depth could be 70% of the value found by the EROS team. The value obtained when only the white dwarf population was considered has been found to be 50% (Camacho et al. 2007). Thus, the simulations presented here reproduce better the results of the EROS experiment. Obviously the red dwarf population is the responsible of this increment. On the other hand, when a non-standard initial mass function is adopted, the results show only marginal differences with respect to those obtained for a white dwarf population, given that in this case the role of red dwarfs is extremely limited. In summary, our results are in fair agreement with those obtained by the EROS experiment, and they seem to indicate that the microlensing optical depth obtained by the MACHO collaboration is an overestimate.

3.4. The dark matter density

With the information obtained so far, we are in position to assess to which extent the mass range the stellar populations discussed here can contribute to the baryonic dark matter halo. Based on their ~ 15 microlensing events, the MACHO collaboration has derived an estimate of the halo fraction of dark matter f as well as the MACHO mass m using maximum-likelihood techniques. A similar analysis has been done by the EROS team, but with the significant difference that, in this case, no event has been reported for the LMC, which means that only an upper limit on the halo mass fraction can be obtained. In order to compare the results of the MACHO and EROS collaborations with our Monte Carlo simulations we have adopted as our reference model the isothermal sphere of core radius 5 kpc with a value of $\rho_0 = 0.0079 M_{\odot} \text{pc}^{-3}$ for the local dark matter density and disregarding the contribution of the LMC halo. For this model we obtain that the optical depth towards the LMC is $\tau_{\text{LMC}} = 5.1 \times 10^{-7} f$. The different estimates of the halo mass fraction f as a function of the mass are plotted in Fig. 5. We show as a solid line the curve of the MACHO 95% confidence level as taken from Alcock et al. (2000) as well as the EROS 95% confidence level upper limit based on no observed events in the EROS-1 and EROS-2 data (Tisserand et al. 2007). Also represented are the individual contribution of each population under study as well as the whole population along with their corresponding 95% confidence level error bars. It is remarkable that the value obtained for the whole halo simulated population is in agreement within the 95% confidence level curves of both observational estimates. Thus, our results predict that the range of stellar masses within 0.08 and $10 M_{\odot}$ provides $f = 0.05$ and an average mass of $0.411 M_{\odot}$ to the halo dark matter in agreement with the currently observational data. This result corroborates our previous estimates about the limited contribution of the CO white dwarfs and the ONe white dwarfs (García-Berro et al. 2004; Camacho et al. 2007).

4. Conclusions

We have extended our previous studies about the contribution to the halo dark matter of the white dwarf population to the Galactic population of red dwarfs. Based on a series of Monte Carlo simulations which incorporate the most up-to-date evolutionary tracks for red dwarfs, CO white dwarfs and ONe white dwarfs and reliable models for our Galaxy and the LMC we have estimated the contribution of these objects to the microlensing optical depth towards the LMC and compared it with that obtained by the MACHO and EROS collaborations. In a first set of simulations we have found that the contribution of the red dwarf population practically doubles the contribution found so far for the white dwarf population. Our results indicate that the whole population of these stars can account at most for a ~ 0.3 of the optical depth found by the MACHO team. This value implies that the contribution of the full range of masses between 0.08 and $10 M_{\odot}$ represents a 5% of the halo dark matter with an average mass of $0.4 M_{\odot}$. Despite that this result is in partial agreement with the 95% confidence level MACHO estimate for a standard isothermal sphere and no halo LMC contribution, the expected number of events obtained by our simulations (3 events at the 95% confidence level) is substantially below the 13 to 17 observed MACHO events. These arguments reinforce the idea, previously pointed out by other studies, that the optical depth found by the MACHO team should be an overestimate, probably due to contamination of self-lensing objects, variable stars

Magnitude	Standard			AL		
	17.5	22.5	27.5	17.5	22.5	27.5
$\langle N_{\text{WD}} \rangle$	0 ± 1	0 ± 1	0 ± 1	1 ± 1	1 ± 1	1 ± 1
$\langle m \rangle (M/M_{\odot})$	0.385	0.384	0.427	0.633	0.637	0.637
$\langle \mu \rangle ('' \text{ yr}^{-1})$	0.020	0.013	0.009	0.028	0.022	0.011
$\langle d \rangle$ (kpc)	2.49	4.26	6.55	1.83	2.39	5.27
$\langle V_{\text{tan}} \rangle$ (km s $^{-1}$)	241	269	267	242	250	266
$\langle t_{\text{E}} \rangle$ (d)	38.3	45.0	54.7	42.6	50.0	75.6
$\langle \tau/\tau_0 \rangle$	0.558	0.695	0.163	0.839	0.628	0.488

Table 4. Summary of the results obtained for the simulation of microlenses towards the LMC for the EROS experiment for an age of the halo of 14 Gyr, different model initial mass functions, and several magnitude cuts.

and others. Moreover, we have assessed the compatibility between the observed event rate distribution and the ones obtained for the different populations under study. Our results show that the CO white dwarf population can reproduce fairly well the observed event rate distribution although, as mentioned earlier, the expected number of events is considerable smaller. On the other hand, the negative results obtained by the EROS team towards the LMC are in agreement with our standard halo simulation. Finally, and for the sake of completeness, we have studied the effects of a log–normal biased initial mass function. In this case, the contribution of the red dwarf population is only marginal given that the production of low–mass stars is strongly inhibited. Accordingly, the total contribution to the microlensing optical depth is not different from that found in previous studies for the white dwarf contribution.

Acknowledgements. Part of this work was supported by the MEC grants AYA05–08013–C03–01 and 02, by the European Union FEDER funds and by the AGAUR.

References

- Adams, F.C., & Laughlin, G., 1996, *ApJ*, 468, 686
- Alcock, C., Allsman, R.A., Alves, D., Axelrod, T.S., Becker, A.C., Bennett, D.P., Cook, K.H., Freeman, K.C., Griest, K., Guern, J., Lehner, M.J., Mashall, S.L., Peterson, B.A., Pratt, M.R., Quinn, P.J., Rodgers, A.W., Stubbs, C.W., Sutherland, W., & Welch, D.L., 1997, *ApJ*, 486, 69
- Alcock, C., Allsman, R.A., Alves, D.R., Axelrod, T.S., Becker, A.C., Bennett, D.P., Cook, K.H., Dalal, N., Drake, A.J., Freeman, K.C., Geha, M., Griest, K., Lehner, M.J., Marshall, S.L., Minniti, D., Nelson, C.A., Peterson, B.A., Popowski, P., Pratt, M.R., Quinn, P.J., Stubbs, C.W., Sutherland, W., Tomaney, A.B., Vandehei, T., & Welch, D., 2000, *ApJ*, 542, 281
- Althaus, L.G., García-Berro, E., Isern, J., Córscico, A.H., & Rohrmann, R.D., 2007, *A&A*, 465, 249
- Baraffe, I., Chabrier, G., Allard, F., & Hauschildt, P.H., 1998, *A&A*, 337, 403
- Becker, A.C., Rest, A., Stubbs, C., Miknaitis, G.A., Miceli, A., Covarrubias, R., Hawley, S.L., Aguilera, C., Smith, R.C., Suntzeff, N.B., Olsen, K., Prieto, J.L., Hiriart, R., Garg, A., Welch, D.L., Cook, K.H., Nikolaev, S., Clocchiatti, A., Minniti, D., Keller, S.C. & Schmidt, B.P., 2005, *IAU Symposium*, 225, 357
- Belokurov, V., Evans, N.W., Le Du, Y., 2003, *MNRAS*, 341, 1373
- Belokurov, V., Evans, N.W., Le Du, Y., 2004, *MNRAS*, 352, 233
- Binney, J., & Tremaine, H., 1987, *Galactic Dynamics* (Princeton: Princeton Univ. Press)
- Calchi Novati, S., de Luca, F., Jetzer, P., & Scarpetta, G., 2006, *A&A*, 459, 407
- Camacho, J., Torres, S., Isern, J., Althaus, L.G., & García-Berro, E., 2007, *A&A*, 471, 151
- Canal, R., Isern, J., & Ruiz-Lapuente, P., 1997, *ApJ*, 488, L35
- Chabrier, G., Segretain, L., & Méra, D., 1996, *ApJ*, 468, 21
- Chabrier, G., 2004, *ApJ*, 611, 315
- Charlot, S., & Silk, J., 1995, *ApJ*, 445, 124
- Cutri, R.M., Skrutskie, M.F., van Dyk, S., Beichman, C.A., Carpenter, J.M., Chester, T., Cambresy, L., Evans, T., Fowler, J., Gizis, J., Howard, E., Huchra, J., Jarrett, T., Kopan, E.L., Kirkpatrick, J.D., Light, R.M., Marsh, K.A., McCallon, H., Schneider, S., Stiening, R., Sykes, M., Weinberg, M., Wheaton, W.A., Wheelock, S., & Zacarias, N., 2003, *2MASS All Sky Catalog of point sources*, Univ. of Massachusetts and IPAC/California Institute of Technology
- Dehnen, W. & Binney, J., 1998, *MNRAS*, 298, 387
- Eisenstein, D.J., Liebert, J., Harris, H.C., Kleinman, S.J., Nitta, A., Silvestri, N., Anderson, S.A., Barentine, J.C., Brewington, H.J., Brinkmann, J., Harvanek, M., Krzesiński, J., Neilsen, E.H., Long, D., Schneider, D.P., & Snedden, S.A., 2006, *ApJS*, 167, 40
- Finley, D.S., Koester, D., & Basri, G., 1997, *ApJ*, 488, 375
- Flynn, C., Holopainen, J., & Holmberg, J., 2003, *MNRAS*, 339, 817
- García-Berro, E., Torres, S., Isern, J., & Burkert, A., 2004, *A&A*, 418, 53
- Gates, E.I., & Gyuk, G., 2001, *ApJ*, 547, 786
- Goldman, B., Afonso, A., Alard, Ch., Albert, J.-N., Amadon, A., Andersen, J., Ansari, R., Aubourg, É., Bareyre, P., Bauer, F., Beaulieu, J.-Ph., Blanc, G., Bouquet, A., Char, S., Charlot, X., Couchot, F., Coutures, Ch., Derue, F., Ferlet, R., Fouqué, P., Glicenstein, J.-F., Gould, A., Graff, D., Gros, M., Haïssinski, J., Hamadache, C., Hamilton, J.-Ch., Hardin, D., Kat, J. de, Kim, A., Lasserre, Th., Le Guillou, L., Lesquoy, É., Loup, C., Magneville, Ch., Mansoux, B., Marquette, J.-B., Maurice, É., Maury, A., Milsztajn, A., Moniez, M., Palanque-Delabrouille, N., Perdureau, O., Prévot, L., Regnault, N., Rich, J., Spiro, M., Tisserand, P., Vidal-Madjar, A., Vigroux, L., & Zylberajch, S., 2002, *A&A*, 389, 69
- Griest, K., 1991, *ApJ*, 366, 412
- Gyuk, G., Dalal, N., & Griest, K., 2000, *ApJ*, 535, 90
- Hambly, N.C., Irwin, M.J., & MacGillivray, H.T., 2001, *MNRAS*, 326, 1295
- Hansen, B.M.S., 1998, *Nature*, 394, 860
- Hansen, B.M.S., & Liebert, J., 2003, *ARA&A*, 41, 465
- Holopainen, J., Flynn, C., Knebe, A., Gill, S.P., & Gibson, B.K., 2006, *MNRAS*, 368, 1209
- Ibata, R.A., Richer, H.B., Gilliland, R.L., & Scott, D., 1999, *ApJ*, 524, L95
- Iben, I., & Laughlin, G., 1989, *ApJ*, 341, 312
- Isern, J., García-Berro, E., Hernanz, M., Mochkovitch, R., & Torres, S., 1998, *ApJ*, 503, 239
- James, F., 1990, *Comput. Phys. Commun.*, 60, 329
- Kallivayalil, N., van der Marel, R.P., Alcock, C., Axelrod, T., Cook, K.H., Drake, A.J., & Geha, M., 2006, *ApJ*, 638, 772
- Kerins, E., & Evans N.W., 1998, *ApJ*, 503, 75
- Kilic, M., Mendez, R.A., Von Hippel, T., & Winget, D.E., 2005, *ApJ*, 633, 1126
- Klypin, A., Zhao, H., & Somerville, R., 2002, *ApJ*, 573, 597
- Knox, R.A., Hawkins, M.R.S., & Hambly, N.C., 1999, *MNRAS*, 306, 736
- Lasserre, T., Afonso, C., Albert, J.N., Andersen, J., Ansari, R., Aubourg, É., Bareyre, P., Bauer, F., Beaulieu, J.P., Blanc, G., Bouquet, A., Char, S., Charlot, X., Couchot, F., Coutures, C., Derue, F., Ferlet, R., Glicenstein, J.F., Goldman, B., Gould, A., Graff, D., Gros, M., Haïssinski, J., Hamilton, J.C., Hardin, D., de Kat, J., Kim, A., Lesquoy, É., Loup, C., Magneville, C., Mansoux, B., Marquette, J.B., Maurice, É., Milsztajn, A., Moniez, M., Palanque-Delabrouille, N., Perdureau, O., Prévot, L., Regnault, N., Rich, J., Spiro, M., Vidal-Madjar, A., Vigroux, L., & Zylberajch, S., 2001, *A&A*, 355, L39
- Liebert, J., Bergeron, P., & Holberg, J., 2005, *ApJS*, 156, 47
- Liebert, J., Dahn, C.C., & Monet, D.G., 1989, in “White Dwarfs”, Ed. G. Wegner (Berlin: Springer), 15
- Lucy, L., 2000, *MNRAS*, 318, 92
- Majewski, S.R., & Siegel, M.H., 2002, *ApJ*, 569, 432
- Mollerach, S., & Roulet, E., 2002, *Gravitational Lensing and Microlensing* (Singapore: World Scientific)
- Muraki, Y., Sumi, T., Abe, F., Bond, I., Carter, B., Dodd, R., Fujimoto, M., Hearnshaw, J., Honda, M., Jugaku, J., Kabe, S., Kato, Y., Kobayashi, M., Koribalski, B., Kilmartin, P., Masuda, K., Matsubara, Y., Nakamura, T., Noda, S., Pennycook, G., Rattenbury, N., Reid, M., Saito, T., Sato, H., Sato, S., Sekiguchi, M., Sullivan, D., Takeuti, M., Watase, Y., Yanagisawa, T., Yock, P. & Yoshizawa, M., 1999, *Progress of Theoretical Physics Supplement*, 133, 233
- Navarro, J.F., Frenck, C.S., & White, S.D.M., 1997, *ApJ*, 490, 493

- Nelson, C.A., Cook, K.H., Axelrod, T.S., Mould, J.R., & Alcock, C., 2002, *ApJ*, 573, 644
- Oppenheimer, B.R., Hambly, N.C., Digby, A.P., Hodgkin, S.T., & Saumon, D., *Science*, 292, 698
- Paczyński, B., 1986, *ApJ*, 304, 1
- Rahvar, S., 2005, *MNRAS*, 356, 1127
- Reylé, C., Robin, A.C., & Créze, M., 2001, *A&A*, L53
- Sahu, K., 1994, *Nature*, 370, 275
- Salaris, M., García-Berro, E., Hernanz, M., Isern, J. & Saumon, D., 2000, *ApJ*, 544, 1036
- Scalo, J., 1998, in “*The Stellar Initial Mass Function*”, Eds.: G. Gilmore & D. Howell (San Francisco: PASP Conference Series), Vol. 142, 201
- Schneider, P., Kochanek, C.S., & Wambsgans, J., 2004, in “*Saas-Fee lectures on Gravitational Lensing*”
- Silk, J., 2007, in “*The invisible universe: dark matter and dark energy*”, Proc. of the Third Aegean Summer School (Berlin: Springer Verlag), Lecture Notes in Physics, Vol. 720, 101
- Tisserand, P., Le Guillou, L., Afonso, C., Albert, J. N., Andersen, J., Ansari, R., Aubourg, E., Bareyre, P., Beaulieu, J. P., Charlot, X., Coutures, C., Ferlet, R., Fouqué, P., Glicenstein, J. F., Goldman, B., Gould, A., Graff, D., Gros, M., Haissinski, J., Hamadache, C., de Kat, J., Lasserre, T., Lesquoy, E., Loup, C., Magneville, C., Marquette, J. B., Maurice, E., Maury, A., Milsztajn, A., Moniez, M., Palanque-Delabrouille, N., Perdureau, O., Rahal, Y. R., Rich, J., Spiro, M., Vidal-Madjar, A., Vigroux, L., & Zylberajch, S., 2007, *A&A*, 469, 387
- Torres, S., García-Berro, E., & Isern, J., 1998, *ApJ*, 508, L71
- Torres, S., García-Berro, E., Burkert, A., & Isern, J., 2002, *MNRAS*, 336, 971
- Udalski, A., Szymanski, M., Kaluzny, J., Kubiak, M., Mateo, M., & Krzeminski, W., 1994, *Acta Astron.*, 44, 1
- Vennes, S., Smith, R.J., Boyle, J., Croom, S.M., Kawka, A., Shanks, T., Miller, L., & Loaring, N., 2002, *MNRAS*, 335, 673
- Vidrih, S., Bramich, D.M., Hewett, P.C. Evans, N.W., Gilmore, G., Hodgkin, S., Smith, M., Wyrzykowski, L., Belokurov, V., Fellhauer, M., Irwin, M.J., McMahon, R.G., Zucker, D., Munn, J.A., Lin, H., Miknaitis, G., Harris, H.C., Lupton, R.H., & and Schneider, D.P., 2007, *MNRAS*, 382, 515
- Zhao, H.S., 1998, *MNRAS*, 294, 139